Research Article | Vol. 11, No. 11 / 1 Nov 2021 / Optical Materials Express 3646
Optical Materials EXPRESS

Wave theory of virtual image [Invited]

ARLEN R. BEKIROV,[1,*] BORIS S. LUK'YANCHUK,[1] ZENGBO WANG,[2] AND ANDREY A. FEDYANIN[1]

[1]Faculty of Physics, Lomonosov Moscow State University, Moscow 119991, Russia
[2]School of Electronic Engineering, Bangor University, Dean Street, Bangor, Gwynedd, LL57 1UT, UK
[*]bekirov@nanolab.phys.msu.ru

Abstract: The super resolution effect with virtual image was discovered about ten years ago using micron-sized transparent spherical dielectric particles. However, within the range of the corresponding size parameters, the simple approximation of geometric optics is not valid. Correct description of the virtual image needs the wave theory. Here we developed a novel theoretical method based on the wave theory of virtual image formation within a transparent dielectric sphere and discussed a few unusual effects arising in the frame of the wave theory.

1. Introduction

The lenses of microscopes and telescopes have a characteristic size R of about centimeter scale. It means that a typical size parameter, $q = 2\pi R/\lambda$, for these devices in the optical range of spectrum exceeds $q >> 10^2$ -10^3 . Magnification M of virtual image within the dielectric sphere at $q > 10^2$ follows well the geometrical optics approximation, $M = n/(2\text{-}n)$ (here n is a refractive index) while the resolution of virtual image in a transparent sphere is restricted by diffraction limit $\Delta x \sim \lambda/2n$. However, with a spheres of some micrometer size and refraction index $n < 2$ it was found experimentally magnification in the range $M = 2$ - 8 [1–18] depending on the refraction index. Resolution is a more complicated problem. Almost all the papers, mention in review [13] show experiments which overcome diffraction limit; however, the experimental resolution limit vary in broad range from $\lambda/2$ till $\lambda/8$. A theoretical description of super resolution effect requires a description of the virtual image within the frame of the wave theory. In the present paper we discuss the theory, suggested in [19], in more detail, including the situations out of the limit of geometrical optics, e.g., at $n \to 2$ where magnification has singularity, $M \to \infty$.

2. Diffraction of an arbitrary wave on a sphere

According to integral Helmholtz-Kirchhoff theorem, the arbitrary field in a free space might be represented as:

$$\mathbf{E}(\mathbf{r}) = \frac{1}{4\pi} \oiint_{\Sigma} \left[G\mathbf{e}^j (\mathbf{n}\cdot\nabla) E_j - E_j \mathbf{e}^j (\mathbf{n}\cdot\nabla) G \right] k^2 dS_o \tag{2.1}$$

where $G = \frac{\exp(ik|\vec{r}-\vec{r}_o|)}{k|\vec{r}-\vec{r}_o|}$, $\nabla = \frac{1}{k}\left\{\frac{\partial}{\partial x_o}, \frac{\partial}{\partial y_o}, \frac{\partial}{\partial z_o}\right\}$ and $k = 2\pi/\lambda$ is the wave number.

The field $\mathbf{E}(\mathbf{r})$ in (2.1) is written as a superposition of two types of sources: $G(\mathbf{r}, \mathbf{r}_o)\mathbf{e}^j$ and $\mathbf{e}^j(\mathbf{n}\cdot\nabla)G(\mathbf{r}, \mathbf{r}_o)$ Despite the fact that for true $\mathbf{E}$ fields should be $div\,\mathbf{E} = 0$, the field in (2.1) is presented by a superposition of sources for each of which $div\,(G(\mathbf{r}, \mathbf{r}_o)\mathbf{e}^j) \neq 0$, and $div\,(\mathbf{e}^j \nabla_i G(\mathbf{r}, \mathbf{r}_o)) \neq 0$. This discrepancy can be avoided if we apply to formula (2.1) an analog of the gauge transformation, $\mathbf{E} \to \mathbf{E} + \nabla^r(\nabla^r \mathbf{E})$, here the operator ∇^r acts on r variables (!), similar to how it is done when calculating the field through the Hertz potentials. Applying this transformation to (2.1) we have

$$\mathbf{E}^{(i)}(\mathbf{r}) = \frac{1}{4\pi} \oiint_{\Sigma} \left[(\mathbf{n},\nabla) E_j^{(i)} \left(G\mathbf{e}^j - \nabla^r \nabla_j^r G \right) - E_j^{(i)} \left((\mathbf{n},\nabla) G\mathbf{e}^j - \nabla^r \nabla_j^r (\mathbf{n},\nabla) G \right) \right] k^2 dS_o \tag{2.2}$$

#437467 https://doi.org/10.1364/OME.437467
Journal © 2021 Received 20 Jul 2021; revised 26 Aug 2021; accepted 26 Aug 2021; published 5 Oct 2021

Optical Materials EXPRESS

The field determined in this manner will be represented as a superposition of purely vortex sources. In principle, such a transformation might be omitted, but in this case, it is necessary to consider the longitudinal modes [19]. Formula (2.2) could be represented in another form:

$$\mathbf{E}^{(i)}(\mathbf{r}) = -\frac{1}{4\pi}\oiint_{\Sigma}\left[i\frac{\mu}{n}\left[\mathbf{n},\mathbf{H}^{(i)}\right]G + i\frac{\mu}{n}\left(\left[\mathbf{n},\mathbf{H}^{(i)}\right],\nabla^r\right)\nabla^r G + \left[\left[\mathbf{n},\mathbf{E}^{(i)}\right],\nabla G\right]\right]k^2 dS_0 \quad (2.3)$$

Representations (2.2) and (2.3) are equivalent in the case of an infinite or closed surface. In the case of a bounded surface, they differ in the contour integral. Let us denote by I_1 the field value calculated by formula (2.2), and I_2 - the field calculated by formula (2.3). According to [20,21] we have the relation

$$I_2 = I_1 + \frac{1}{4\pi}\oint_{C}\left[[\mathbf{E}^{(i)},\mathbf{s}]G + \nabla^r(\nabla^r,\,[\mathbf{E}^{(i)},\mathbf{s}]G)\right]k\,dl_o \quad (2.4)$$

Here $\mathbf{s}$ is the direction vector of the contour element dl_o. This contour integral plays the dominant role in definition of the optical resolution in the virtual image. Although representations (2.3) and (2.2) are equivalent, if we calculate the limiting value of the field on the plane $\sum$ and then substitute this value in (2.2). Thus (2.2) and (2.3) correspond to different approximations for the field in the plane.

Diffraction of an arbitrary field on a sphere can be presented as a superposition of solutions for point sources. In general case, the solution has the form (the fields $\mathbf{E}^{(1)}$, $\mathbf{E}^{(2)}$ are the solutions in space outside and inside the particle):

$$\mathbf{E}^{(1)} = \mathbf{E}^{(i)} + \sum_{\ell,m}^{\infty} A^{(c)}_{\ell m}\mathbf{N}^{(c)}_{\ell m} + A^{(s)}_{\ell m}\mathbf{N}^{(s)}_{\ell m} + B^{(c)}_{\ell m}\mathbf{M}^{(c)}_{\ell m} + B^{(s)}_{\ell m}\mathbf{M}^{(s)}_{\ell m} \quad (2.5a)$$

$$\mathbf{E}^{(2)} = \sum_{\ell,m}^{\infty} D^{(c)}_{\ell m}\mathbf{N}^{(c)}_{\ell m} + D^{(s)}_{\ell m}\mathbf{N}^{(s)}_{lm} + C^{(c)}_{\ell m}\mathbf{M}^{(c)}_{\ell m} + C^{(s)}_{\ell m}\mathbf{M}^{(s)}_{lm} \quad (2.5b)$$

Here $\mathbf{M}$ and $\mathbf{N}$ are vector spherical harmonics [22]. We seek a solution for functions (2.5) in the form (2.3). We will denote the corresponding scattering coefficients by small symbols. Let x be one of the coefficients $\{a,\, b\}$, $\{c,\, d\}$ for the scattered field and the internal field, respectively. Let ${}^j x^{(c/s)}_{lm}(\mathbf{r}_o)$ is the solution for the source $(G\mathbf{e}^j - \nabla^r\nabla^r_j G)$ in (2.2), and ${}^j_i x^{(c/s)}_{lm}(\mathbf{r}_o)$ is the solution for the source $\mathbf{e}^j\nabla_i G - \nabla^r\nabla^r_j(\nabla_i G)$. Similarly, for $X = \{A,\, B\}$, $\{C,\, D\}$, due to linearity, we obtain

$$X^{(s/c)}_{\ell m} = \frac{1}{4\pi}\oiint_{\Sigma}\left((\mathbf{n},\nabla)\,E_j\,{}^j x^{(c/s)}_{\ell m} - E_j n^{(i)}\,{}^j_i x^{(c/s)}_{\ell m}\right)k^2 dS_o. \quad (2.6)$$

Here E_j are the components of the incident field $\mathbf{E}^{(i)}$ (index i remains omitted for brevity), a similar solution might be written for (2.3). The integration surface in (2.6) can be chosen arbitrarily. See the details of calculations in the Supplement 1.

3. Wave theory of the image

The history of optical imaging constitutes a fascinating stage in the development of optics. In 1609, Galileo invented a two-lens telescope, in which a concave diffusing lens formed an imaginary, magnified image of an object. Among the discoveries made by Galileo with this telescope were sunspots, which he demonstrated in Rome in the spring of 1611. It is thought that in the course of these observations, Galileo spoiled his vision, since the virtual image cannot be

Optical Materials EXPRESS

projected onto the screen. In contrast, the Kepler's telescope, invented by him in 1611, can be converted into a projection device for showing the image of the sun on a screen. Scheiner used this scheme for observing sunspots in the same 1611 and fought with Galileo for the priority of the discovery. In fact, sunspots were known long before Galileo [23]. They may be seen even with the naked eye looking at the Sun through the soot smoked glass.

Kepler in his works of 1611 outlined the rules for constructing an optical image in a lens by ray tracing method. The development of geometric optics after Kepler has been completed two hundred years later, when the laws of geometric optics were taken from the wave optics in the eikonal approximation [24]. Hamilton proved that geometric optics is the limiting case of wave optics for short wavelengths [25]. An analysis of scattering by a sphere [26] showed that, for example, for the refractive index $n = 1.5$, the geometric optics approximation coincides with a high accuracy with the results of the Mie theory at $q = 2\pi R/\lambda \geq 100$. In [19], a procedure was proposed for constructing a virtual converging electromagnetic wave when considering a complex conjugate field. The image field E_{im} was defined as

$$\mathbf{E}_{im} = \frac{1}{4\pi} \iint\limits_{\Gamma} (G(\mathbf{n}, \nabla)\mathbf{E}^*_{se} - \mathbf{E}^*_{se}(\mathbf{n}, \nabla)G)\, k^2 dS. \tag{3.1}$$

Here Γ is some infinite surface homotopic to the plane, $\mathbf{E}_{se}$ is the field emanating from the sources. One can also take Γ as the closed surface surrounding the field sources. Integral (3.1) does not depend on the position and shape of the surface. Field (3.1) can be equivalently represented in the form of the Fourier transform (see details in Supplement 1)

$$\mathbf{E}_{im}(x, y, z) = \frac{1}{(2\pi k_o)^2} \iint\limits_{k_x^2 + k_y^2 \leq k_o^2} \tilde{\mathbf{E}}^*_{se}(k_x, k_y, z_o) e^{-i(k_x x + k_y y + k_z(z - z_o))} dk_x dk_y \tag{3.1a}$$

Here $\tilde{\mathbf{E}}_{se}$ is the two-dimensional Fourier transform field in the xy plane at $z = z_0$, $k_z^2 = k_o^2 - k_x^2 - k_y^2$. It follows from the equivalence of (3.1) and (3.1a) that transformation (3.1) actually reconstructs the field from the source within the spectral range k_0. According to angular spectrum representation, the collected waves have being decomposed into plane waves, which will then numerically propagate backward in the negative z direction to form a virtual image on the image plane [27]. Difference in between of (3.1a) and classical formula is related to range of integration over k_x and k_y, i.e., $k_x^2 + k_y^2 \leq k_o^2$. This difference led to diffusion of virtual image, caused by diffraction.

Following are a few examples. Consider a point source of the following form:

$$\Delta \mathbf{E}_{se} + k^2 \mathbf{E}_{se} = \mathbf{U}, \quad \mathbf{U} = -4\pi k^{-1} (\mathbf{e}_{\perp}, \nabla) \delta(\vec{r} - \vec{r}_o)\mathbf{K} \tag{3.2}$$

where $\mathbf{e}_{\perp}$ is orthogonal to the contour on which the surface Γ is rests, $\mathbf{K}$ is some arbitrary vector. Using the spectral expansion for the Green's function of the wave equation G and (3.1a) one can obtain

$$\mathbf{E}_{im} = \frac{J_1(k\rho)}{k\rho} \mathbf{K}^*, \; z = z_o \tag{3.3}$$

Here $\vec{\rho} = \vec{r}_o - \vec{r}$. In the case of a vortex source of the form $\mathbf{U} \to \mathbf{U} + grad(div\ \mathbf{U})/k^2$, we obtain instead of (3.3)

$$\mathbf{E}_{im} = \frac{J_1(k\rho)}{k\rho} \mathbf{K}^* - \frac{J_2(k\rho)}{k\rho} (\mathbf{K}^*_{\perp} + 2K^*_z \mathbf{e}_z) + \frac{J_3(k\rho)}{k\rho} \frac{(\rho, \mathbf{K}^*)\rho}{\rho^2} - i \frac{j_2(k\rho)}{k\rho} \left(\frac{(\rho, \mathbf{K}^*)}{\rho} \mathbf{e}_z + K^*_z \frac{\rho}{\rho} \right), \; z = z_o \tag{3.4}$$

Similarly, in the case of a source of the form $\Delta \mathbf{E}_{se} + k^2 \mathbf{E}_{se} = \mathbf{U} + grad(div\ \mathbf{U})/k^2$, $\mathbf{U} = -4\pi k^{-1} \delta(\vec{r} - \vec{r}_o)\mathbf{K}$, we have

$$\mathbf{E}_{im} = -i \left(j_0(k\rho)\mathbf{K}^* - \frac{j_1(k\rho)}{k\rho} \mathbf{K}^* + j_2(k\rho) \frac{(\rho, \mathbf{K}^*)\rho}{\rho^2} \right) - \frac{J_2(k\rho)}{k\rho} \left(\frac{(\rho, \mathbf{K}^*)}{\rho} \mathbf{e}_z + K^*_z \frac{\rho}{\rho} \right), \; z = z_o \tag{3.5}$$

Optical Materials EXPRESS

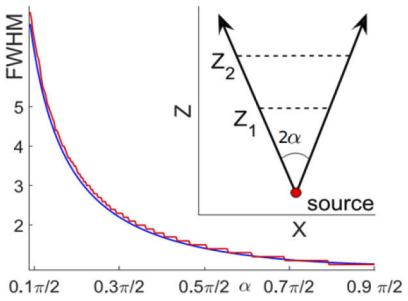

Fig. 1. Comparison of the point source image half-width (red line) with $1/\sin\alpha$ (blue line). The inset shows the geometry of the calculation. The result does not change when going from Z1 to Z2.

Here J_n are the Bessel functions and j_n are the spherical Bessel functions. We pay attention that the formulas (3.3–3.5) are valid only on plane $z = z_o$. If we choose a bounded integration surface Γ, then the image of (3.2) will broaden in accordance with the formula $1/\sin\alpha$, see in Fig. 1. A similar picture takes place for the delta source. This correspondence will be maintained only when the distance to the source is much greater λ . In this case, the integral in (3.1) does not change with a change in the integration surface Γ within a given solid angle. The virtual field (3.1) is consistent with the classical concepts of optical resolution. This makes it possible to understand Γ as the aperture of an optical device.

The above results of this paragraph refer to the case of free space, without a sphere. Next, we move on to consider the effects associated with the presence of a sphere. In the experiments with superresolution [1–6] a virtual image in a sphere obtained from closely spaced slits is usually considered. The wave theory of such an image was developed in [19]. To calculate the field, one can use any of the formulas (2.2–2.3), provided that the exact expression for the field in the plane of the screen is known. Strictly speaking, to find this field, an integral equation should be solved

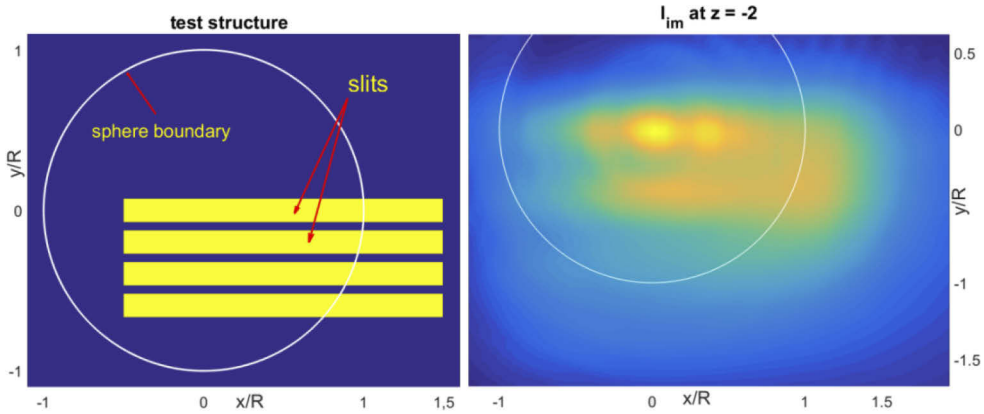

Fig. 2. Calculated virtual image of four adjacent slits. The geometry on left figure the similar as [1], 360-nm-wide lines spaced 130 nm apart, wavelength 600 nm, diameter microsphere 4.96 μm. The field of view at $z/R = -2$ permits to see just two strips but with higher magnification. The figure shows that the four strips are not distinguishable, it also emerged as one at the "border" of the array of spheres. The strips are visible only inside this array, we believe that the visibility of the four strips is due to the fact that it is inside the array of spheres, in contrast to our consideration with a single isolated sphere. Note, that the polarization of the field within the slit also influences resolution [36].

Optical Materials EXPRESS

(see, for example, [28]). The commonly used Kirchhoff approximation (constant field inside the slit) differs both from the distribution for wide slits known in diffraction theory (see, for example, the limiting case of diffraction at the edge of the screen [28,29]) and from the distribution at small apertures [28,30–32]. An experimental study [33] shows that the field maxima are formed either at the edge of the slit or in its middle, depending on the width of the slit. We used approximate expressions in our calculations with the field amplitude increasing at the edge of the slot. We chose the fields **E** and **H** in formula (2.3) so that the slits were indistinguishable in their image based on formula (3.1) in the absence of a sphere. In this case, field (3.1) was an even plateau without pronounced maxima. Note that the sensitivity to the shape of the field distribution is related to the contour integral in (2.4). Another important effect is light scattering due to reflection from the metal shield. This effect was considered in the problem "particle on a substrate" [34,35]. In our calculations, it was seen that this effect does not significantly affect the resolution, but significantly affects the observed picture contrast. In particular, if we do not consider the reflection from the screen, the "flare" in Fig. 2 turns out to be so bright that it overlaps the images of the slits. Finally, we considered that the fields inside the gap are coherent only on the scales less than $1.22\,\lambda / 2$. The final result of the calculations is shown in Fig. 2.

Thus, it can be expected that the superresolution effect is associated with the specific features of the behavior of the field inside the slot. This mechanism can be interpreted as follows. Taking into account the features of the near field in the slit, the sphere collects evanescent waves in the near field and effectively transmits them to the far field, which makes it possible to overcome the diffraction limit. Unfortunately, this explanation does not describe superresolution for very small objects, such as nanopores with diameters on the order of $\lambda/10$. It is likely that there must be another mechanism affecting resolution. In particular, holes should probably be considered when reflecting from a plane. In our work, we considered reflection from a solid screen.

We now turn to the Magnification problem. Geometric optics at values of the refractive index close to two, i.e., $n = 2$, leads to singularities in which the virtual image is projected to infinity, where the corresponding magnification factor also goes to infinity. The corresponding formula for magnification is given by

$$M = \frac{\varepsilon \sec\psi}{\varepsilon + (1+\delta)\tan\psi}, \quad \psi = 2\left(\arcsin\varepsilon - \arcsin\frac{\varepsilon}{n}\right) \tag{3.6}$$

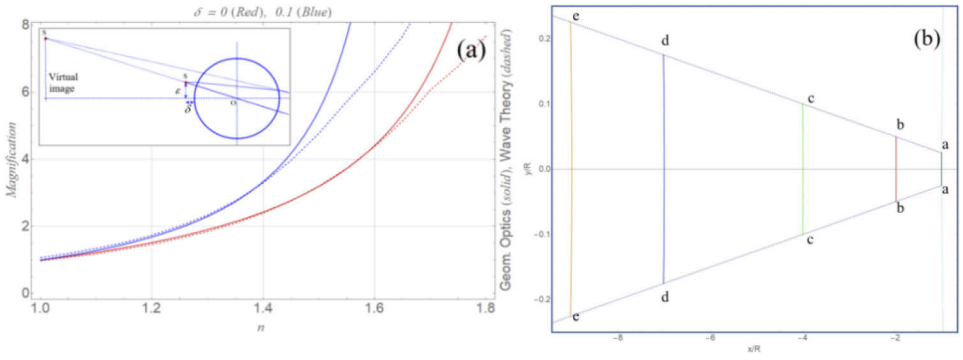

Fig. 3. (a) Magnification versus refractive index according to the geometrical optics approximation – Eq. (3.6) (solid lines) and according to the wave theory – Eq. (2.2) (dashed). Insert shows position of the point source – parameters δ and ε. Geometrical optics curves are computed for $\varepsilon = 0.22$, $\delta = 0$ (red) and $\varepsilon = 0.42$ and $\delta = 0.1$ (blue). (b) Magnification of *a*-*a* line segment at $n = 1.33$ (*b*-*b*), $n = 1.6$ (*c*-*c*), $n = 1.75$ (*d*-*d*), $n = 1.8$ (*e*-*e*). Coordinate x/R indicates position of virtual image.

Optical Materials EXPRESS

Parameters δ and ε set the position of the point source S (see inset in Fig. 3). One can see from Fig. 3(a) characteristic range of applicability of geometrical optics approximation (e.g., $n \leq 1.6$ for $\delta = 0$). Calculations according to the wave theory have been made with $\varepsilon = 0$ and the best fitting of theoretical curves was done with approximation (3.6). Fig.3b shows magnification of a-a line segment situated on the surface of the particle $\delta = 0$, $\varepsilon = \pm 0.025$ at the different refractive index values.

A more difficult problem is to analyze the magnification as a function of the sphere size or a size parameter. Experiments do not give a clear conclusion about the nature of this relationship. The inset in Fig. 4 shows the experimental dependence $M = M(D)$ [17], which indicates an increase in "noise" with an increase in the size of the sphere. In this region of parameters, theoretical calculations according to our model show a large number of optical resonances, see Fig. 4. Naturally for white light, these oscillations are smoothed [37].

Passing from the approximation of geometric optics to wave theory, it is useful to turn to the picture of Huygens wave fronts. In the case of a point source in vacuum, these are the fronts of diverging spherical waves. When crossing the sphere located near the source, the wave fronts are distorted. These distortions depend on the refractive index and the size of the

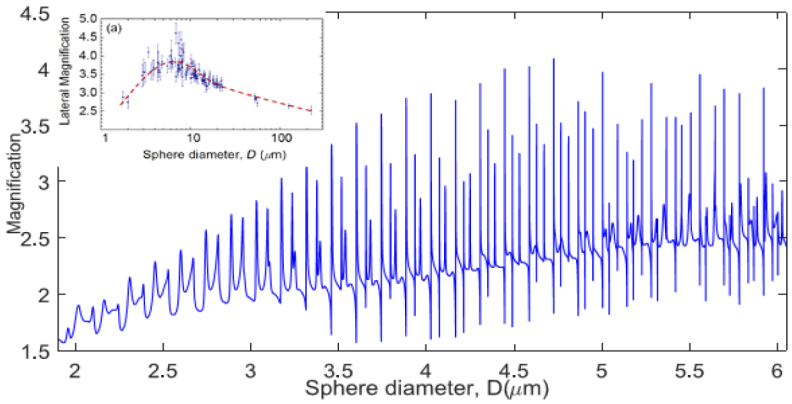

Fig. 4. Optical resonances in magnification versus particle diameter in mm. Refractive index of the particle was n=1.4599, $\lambda = 600$ nm. Insert shows experimental dependence of magnification $M = M(D)$ from Ref. 17.

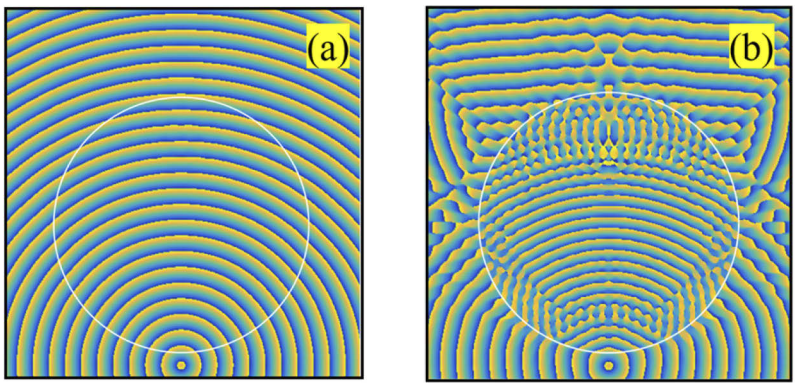

Fig. 5. Spherical wave fronts propagating from the point source situated at the distance $\delta = 0.1R$ from the surface below the sphere with size parameter $q = 50$. Refractive index $n = 1.02$ (a) and $n = 1.5$ (b).

Optical Materials EXPRESS

sphere, Fig. 5. To construct a virtual image, one should create a picture of a converging intensity distribution, starting from the distorted wavefronts at the exit from the sphere. In the case of geometrical optics, an enlarged two-dimensional picture of the original object appears in the "image plane", Fig. 3(b). In the case of the wave theory, the "image plane" is blurred into a certain three-dimensional distribution of light intensity, the delta-shaped point source turns into a "luminous volume", see in Fig. 6.

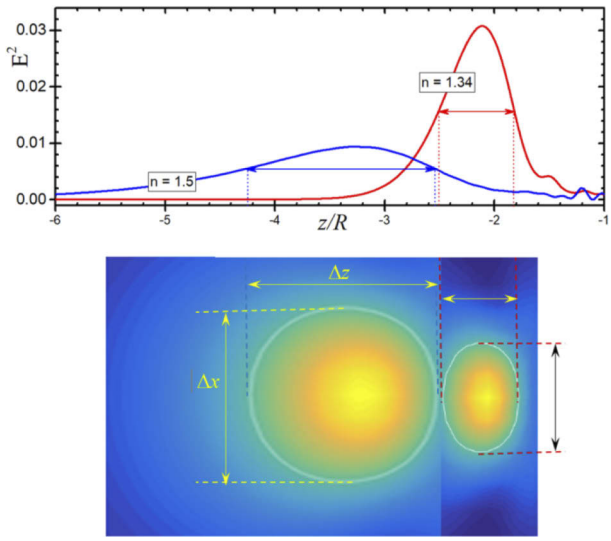

Fig. 6. Distribution of intensity of virtual image of the point source situated at the distance $\delta = 0.1R$ along the z-axis at below the sphere with size parameter $q = 50$. Typical modification of the full width at half maximum (FWHM) distribution shows the growth of a "luminous volume" of virtual image versus refractive index due to increased magnification factor at larger refractive index.

Considering special case with $n = 2$, which is not described in terms of geometric optics. Low-intensity oscillation images could be seen following our wave theory model, This oscillation effect is observed in the range of sufficiently large dimensions (e.g., $q > 20$); with increasing q the intensity of the imaginary field tends to zero, as shown in Fig. 7.

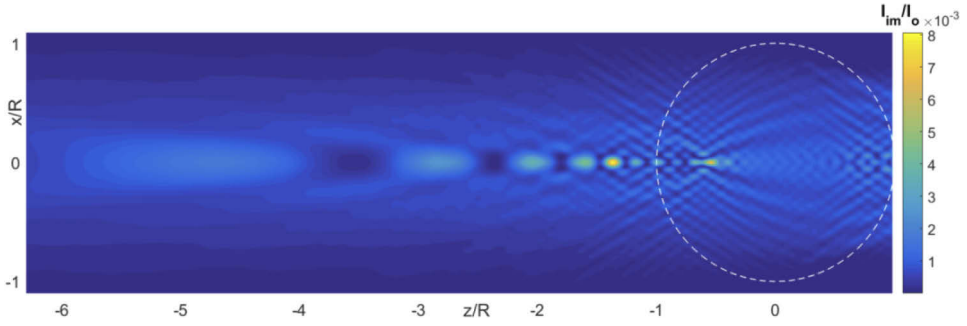

Fig. 7. Distribution of intensity in virtual image for $n = 2$ (singular case in geometric optics) and size parameter $q = 66$. Position of a point source is $\varepsilon = 0$ and $\delta = 0$. I_0 is the intensity of image in case n = 1 (no sphere). A white dashed line shows the position of sphere.

Finally, we will point out one qualitative effect - inversion about the center in the virtual image (transformation $r,\ (x, y) \rightarrow -r,\ (-x, -y)$). At a distance corresponding to the position of

Optical Materials EXPRESS

the virtual image (in the geometric optics approximation, $z = nR/(2-n)$), we see an enlarged picture of the test structure with the maximum magnification M and symmetry corresponding to the original test structure. When the focus position changes from the value and approaches the real plane of the object, $z \to -R$, one can observe an inverted image corresponding to the point symmetry group C_{nv} [38] (a group of rotations around the axis of the n-th order and n reflections in vertical planes). Such symmetry for odd n looks like " pseudo rotation ", see Fig. 8. A phenomenon of this type was observed in the experiment (see Fig. 3 in article [1]). Here the important role plays the coherence of light passing through the star.

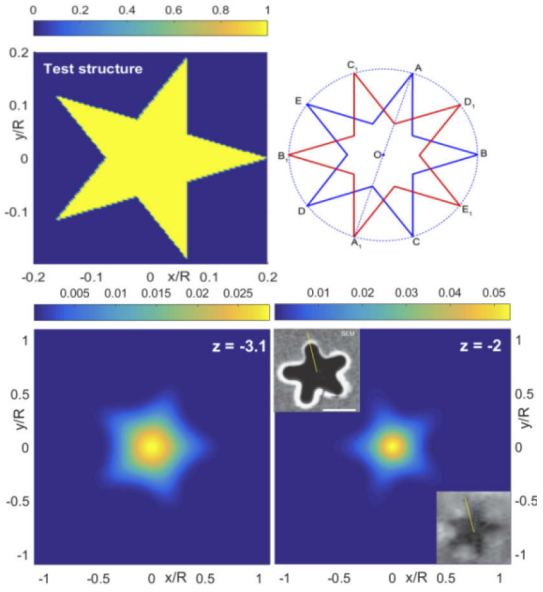

Fig. 8. The top left picture corresponds to the test structure (a star cut in a metal plate). The top right picture illustrating a symmetry transformation in which each point is mirrored relative to the center O ($A \to A_1$, $B \to B_1, \ldots$). (This transforms a blue-lined star into a red-lined star. The bottom left and right pictures show a virtual image of a star at distances $z \approx -3.1R$ (maximum magnification) and $z \approx -2R$ (lower magnification factor, compare Fig. 3(b)). The blurring of the image due to diffraction is also accompanied by its "rotation." In the calculations, we used the values of refractive index $n = 1.5$ and the size parameter $q = 50$. Top insert shows the original star image in the experiment [1]. Down insert shows the virtual image in the dielectric sphere. Corresponding angle of "rotation" is shown by dashed lines.

The origin of "rotation" can be understood starting from formula (3.1a). For a symmetric object in the scattered field, there remain modes with a certain parity in the orbital number m. Formula (3.1a) is invariant under the transformation $(x, y) \to (-x, -y)$ and $(k_x, k_y) \to (-k_x, -k_y)$. For the x-component the explicit form of this formula for a virtual image is:

$$E^*_{im}(x,y,z) = \frac{1}{(2\pi)^2} \iint\limits_{k_x^2+k_y^2 \le k_o^2} \left[\sum_{l,m}^{\infty} A_{lm} \tilde{N}_x^{lm}(k_x,k_y,k_z) + B_{lm} \tilde{M}_x^{lm}(k_x,k_y,k_z) \right] e^{ik_z z_o} e^{i(k_x x + k_y y + k_z(z-z_o))} \frac{dk_x dk_y}{k_o^2} \tag{3.7}$$

(We use E* to shorten the notation of formulas) Let us make the replacement in this formula $(x, y) \to (-x, -y)$ and $(k_x, k_y) \to (-k_x, -k_y)$ and use the properties of the two-dimensional Fourier transform for vector spherical functions. We get the transformed formula

$$E^*_{im}(-x,-y,z) = \frac{1}{(2\pi)^2} \iint\limits_{k_x^2+k_y^2 \le k_o^2} \left[\sum_{l,m}^{\infty} (-1)^{m+1} (A_{lm} \tilde{N}_x^{lm}(k_x,k_y,k_z) + B_{lm} \tilde{M}_x^{lm}(k_x,k_y,k_z)) \right] e^{ik_z z_o} e^{i(k_x x + k_y y + k_z(z-z_o))} \frac{dk_x dk_y}{k_o^2} \tag{3.8}$$

Optical Materials EXPRESS

In the presence of modes of a certain parity in m, expression (3.8) differs from (3.7) only in sign. The change in the virtual image occurs when the parameter z corresponding to the plane of the virtual image changes, $z < 0$. The parameter z_0 in formulas (3.7), (3.8) does not play any role. We have kept it to denote the continuity of these formulas with (3.1). As $\tilde{\mathbf{E}}_{se}(k_x, k_y, z_o) \propto e^{ik_z z_0}$ then the dependence on z_0 in the formulas disappears. From (3.8) it follows that the inversion with respect to "rotation" takes place only for odd $m = 2p + 1$. Such symmetry exists only for structures with symmetry C_{2p+1}, for example, for an equilateral triangle or a star. At the same time, for structures with ellipse or square symmetry, no "rotation" occurs in the virtual image because with a given symmetry, they pass into themselves.

4. Conclusion

The construction of an imaginary image in classical optics has been studied since the time of Galileo, in whose telescope the concave diffusing lens formed an imaginary, magnified image of the object. For particles with a size of the order of several light wavelengths λ, the geometric optics approximation does not work, and it is necessary to use the wave theory of an imaginary image. For random reasons, this theory turned out to be a blank spot on the map of classical optics. The experimental investigation and theoretical discussion shows that the virtual image in micrometer size particles permits to resolve structures below the diffraction limit, e.g., $\lambda/6$ and less. The theoretical limit of resolution also depends on the particle on surface effect, coherence and exact field distribution within the slit. Experiments shows resolution on the level $\lambda/8$ in white light, i.e., structures with size of about 50 nm were resolved, see e.g. in Ref. [1].

Funding. «BASIS» Foundation (#20-2-1-51-1); Royal Society grants (IEC\NSFC\181378, IEC\R2\202178); European ERDF (CPE 81400, SPARCII c81133); Russian Foundation for Basic Research (20-02-00715, 21-58-10005); Russian Science Foundation (20-12-00389); Ministry of Science and Higher Education of the Russian Federation (14.W03.31.0008).

Disclosures. The authors declare no conflicts of interest.

Data availability. Data underlying the results presented in this paper are available in Ref. [1].

Supplemental document. See Supplement 1 for supporting content.

References

1. Z.B. Wang, W. Guo, L. Li, B. Luk'yanchuk, A. Khan, Z. Liu, Z. Chen, and M. H. Hong, "Optical virtual imaging at 50 nm lateral resolution with a white light nanoscope," Nat Commun **2**, 1 (2011).
2. A. Darafsheh, G. F. Walsh, L. Dal Negro, and V. N. Astratov, "Optical super-resolution by high-index liquid immersed microspheres," Appl. Phys. Lett. **101**(14), 141128 (2012).
3. S. Lee, L. Li, Y. Ben-Aryeh, Z. Wang, and W. Guo, "Overcoming the diffraction limit induced by microsphere optical nanoscopy," J. Opt. **15**(12), 125710 (2013).
4. L. A. Krivitsky, J. J. Wang, Z. Wang, and B. Luk'yanchuk, "Locomotion of microspheres for super-resolution imaging," Sci. Rep. **3**(1), 3501 (2013).
5. A. Darafsheh, N. I. Limberopoulos, J. S. Derov, D. E. Walker Jr, and V. N. Astratov, "Advantages of microsphere assisted super-resolution imaging technique over solid immersion lens and confocal microscopies," Appl. Phys. Lett. **104**(6), 061117 (2014).
6. H. Cang, A. Salandrino, Y. Wang, and X. Zhang, "Adiabatic far-field sub-diffraction imaging," Nat Commun **6**(1), 7942 (2015).
7. A. Darafsheh, C. Guardiola, A. Palovcak, J. C. Finlay, and A. Cárabe, "Optical super-resolution imaging by high-index microspheres embedded in elastomers," Opt. Lett. **40**(1), 5–8 (2015).
8. H. Yang, R. Trouillon, G. Huszka, and M. A. M. Gijs, "Super-resolution imaging of a dielectric microsphere is governed by the waist of its photonic nanojet," Nano Lett. **16**(8), 4862–4870 (2016).
9. V.N. Astratov, A.V. Maslov, K.W. Allen, N. Farahi, Y. Li, A. Brettin, N. I. Limberopoulos, Jr. D. E. Walker, A. M. Urbas, V. Liberman, and M. Rothschild, "Fundamental limits of super-resolution microscopy by dielectric microspheres and microfibers," Proc SPIE **9721**, 97210K (2016).
10. F. Wang, L. Liu, P. Yu, Z. Liu, H. Yu, Y. Wang, and W. J. Li, "Three-dimensional super-resolution morphology by near-field assisted white-light interferometry," Sci. Rep. **6**(1), 24703 (2016).
11. Z. Wang, "Microsphere super-resolution imaging," Nanoscience **3**, 193–210 (2016).
12. H. S. S. Lai, F. Wang, Y. Li, B. Jia, L. Liu, and W. J. Li, "Super-resolution real imaging in microsphere-assisted microscopy," PLoS One **11**, e0165194 (2016).

Optical Materials EXPRESS

13. B. S. Luk'yanchuk, R. Paniagua-Domínguez, I. Minin, O. Minin, and Z. Wang, "Refractive index less than two: photonic nanojets yesterday, today and tomorrow," Opt. Mater. Express **7**(6), 1820–1847 (2017).
14. G. Huszka, H. Yang, and M. A. M. Gijs, "Microsphere-based super-resolution scanning optical microscope," Opt. Express **25**(13), 15079 (2017).
15. S. Zhou, Y. Deng, W. Zhou, M. Yu, H. P. Urbach, and Y. Wu, "Effects of whispering gallery mode in microsphere super-resolution imaging," Appl. Phys. B **123**(9), 236 (2017).
16. Z. B. Wang and B. Luk'yanchuk, "Super-resolution imaging and microscopy by dielectric particle-lenses" Chapter 15 in *Label-Free Super-resolution Microscopy* (Springer, 2019), pp. 371–400 .
17. L. Chen, Y. Zhou, Y. Li, and M. Hong, "Microsphere enhanced optical imaging and patterning: from physics to applications," Appl. Phys. Rev. **6**(2), 021304 (2019).
18. J. Zhou, B. Zeng, S. Bi, and Y. Wang, "Enhanced magnification factors in super-resolution imaging using stacked dual microspheres," J. Opt. **22**(8), 085605 (2020).
19. A. R. Bekirov, B. S. Luk'yanchuk, and A. A. Fedyanin, "Virtual image within a transparent dielectric sphere," JETP Lett. **112**(6), 341–345 (2020).
20. J. A. Stratton, *Electromagnetic Theory*, Sec. 8.15 (John Wiley & Sons, 2007).
21. J. D. Jackson, *Classical Electrodynamics*, Third Edition, Chapter 10 (John Wiley & Sons, 2007).
22. C. F. Bohren and D. R. Huffman, *Absorption and Scattering of Light by Small Particles* (John Wiley & Sons, 2008).
23. *Sunspot*, https://en.wikipedia.org/wiki/Sunspot
24. M. Born and E. Wolf, *Principles of Optics* (Cambridge University, 1999).
25. Y. A. Kravtsov and Y. I. Orlov, *Geometrical Optics of Inhomogeneous Media* (Springer, 1990).
26. J. Kofler and N. Arnold, "Axially symmetric focusing as a cuspoid diffraction catastrophe: Scalar and vector cases and comparison with the theory of Mie," Phys. Rev. B **73**(23), 235401 (2006).
27. Y. Duan, G. Barbastathis, and B. Zhang, "Classical imaging theory of a microlens with super-resolution," Opt. Lett. **38**(16), 2988–2990 (2013).
28. H. A. Bethe, "Theory of diffraction by small holes," Phys. Rev. **66**(7-8), 163–182 (1944).
29. N.A. Kirichenko, *Principle of Optics* (Moscow Institute of Physics and Technology, 2016), in Russian.
30. L. Martín-Moreno, F. J. García-Vidal, H. J. Lezec, K. M. Pellerin, T. Thio, J. B. Pendry, and T. W. Ebbesen, "Theory of extraordinary optical transmission through subwavelength hole arrays," Phys. Rev. Lett. **86**(6), 1114–1117 (2001).
31. C. Genet and T. W. Ebbesen, "Light in tiny holes," Nature **445**(7123), 39–46 (2007).
32. F. J. Garcia-Vidal, L. Martin-Moreno, T. W. Ebbesen, and L. Kuipers, "Light passing through subwavelength apertures," Rev. Mod. Phys. **82**(1), 729–787 (2010).
33. Y. Xie, A. R. Zakharian, J. V. Moloney, and M. Mansuripur, "Transmission of light through slit apertures in metallic films," Opt. Express **12**(25), 6106–6121 (2004).
34. P. A. Bobbert and J. Vlieger, "Light scattering by a sphere on a substrate," Physica A: Statistical Mechanics and its Applications **137**(1-2), 209–242 (1986).
35. B. S. Luk'yanchuk, Y. W. Zheng, and Y. F. Lu, "Laser cleaning of solid surface: optical resonance and near-field effects," Proc. SPIE **4065**, 576–587 (2000).
36. V. M. Sundaram and S. B. Wen, "Analysis of deep sub-micron resolution in microsphere-based imaging," Appl. Phys. Lett. **105**(20), 204102 (2014).
37. B. S. Luk'yanchuk, N. Arnold, S. M. Huang, Z. B. Wang, and M. H. Hong, "Three-dimensional effects in dry laser cleaning," Appl. Phys. A **77**(2), 209–215 (2003).
38. L.D. Landau and E.M. Lifshitz, *Quantum Mechanics: Non-relativistic Theory*, § 93 (Elsevier, 2013)